Materials Research Proceedings **4** (2018) 59-64 doi: http://dx.doi.org/10.21741/9781945291678-9

Influence of Laser Power and Traverse Speed on Weld Characteristics of Laser Beam Welded Ti-6Al-4V Sheet

P.M. Mashinini[1,a*] and D.G. Hattingh[2,b]

[1]University of Johannesburg, Department of Mechanical and Industrial Engineering Technology, Doornfontein Campus, Johannesburg, South Africa

[2]Nelson Mandela University, Department of Mechanical Engineering, North Campus, Summerstrand, Port Elizabeth, South Africa

[a]mmashinini@uj.ac.za, [b]danie.hattingh@mandela.ac.za

Keywords: Laser Beam Welding, Ti-6Al-4V, Traverse Speed, Microstructure, Residual Stress

Abstract. In this paper laser beam welding was used for joining 3 mm Ti-6Al-4V alloy sheets in a full penetration butt-weld configuration. Laser beam power and traverse speed were the only parameters varied in an attempt to characterize the influence on weld integrity with specific reference to residual stress and microstructural modifications. The iXRD residual stress data showed a definite influence of traverse speed on residual stresses, with low traverse speeds resulting in an increased tensile residual stresses in the longitudinal direction of the weld whilst in the transverse direction residual stress revealed a more compressive stress state. The residual stress data for this experiment compared favourably with published residual stress data done by synchrotron X-ray diffraction. Weld joint integrity was further analyzed by evaluating the microstructure transformation in the weld nugget. These results revealed a degree of grain growth and the presences of fine acicular β (needle-like α) in prior β grain boundaries with increased traverse speed. Grain growth was predominantly influenced by the cooling rate which is associated with traverse speed. Additionally, the α -phase and β -phase were characterized in the various weld zones by electron backscatter diffraction (EBSD).

Introduction

Laser Beam Welding (LBW) as a fusion joining technique which was invented in the late 1960s [1], has successfully been utilized to weld light metal alloys including aluminium, magnesium and titanium [1, 2]. LBW can be used to weld linear or rotational joints using a carbon dioxide (CO_2) laser. Alternatively, complex joints can be made using a neodymium-doped yttrium aluminium garnet (Nd:YAG) laser [2, 3, 4]. During LBW, a high power laser is focused on the material weld joint-line (typically 1 kW to 5 kW) [2, 5]. LBW process involves heat conduction and heat absorption on the workpiece on the joint-line. This causes material to melt. The temperature increases above the boiling point of the parent material. The vapour pressure increases, creating a narrow capillary (keyhole) which propagates through the material. The keyhole traps almost all the laser power. The keyhole is then filled with metallic vapour as the laser beam traverses, forming a welded joint [6, 7].

Literature has shown some research has been done on LBW processing and it is a growing field. Liu *et al*. [8] reported research work on fatigue damage evolution on pulsed Nd:YAG Ti-6Al-4V laser welded joints. The results indicated a martensitic (α') phase and an underfill flaw in the weld nugget [8]. The results are similar those reported by Xu *et al*. [9] on microstructure characterization of laser welded Ti-6Al-4V fusion zones. The results predominantly showed the

Materials Research Proceedings **4** (2018) 59-64 doi: http://dx.doi.org/10.21741/9781945291678-9

martensitic (α') phase with α and retained β phase. The cooling rate was the main source of phase transformation in the weld nugget, that is, high traverse speed gives high cooling rate [9, 10].

Currently, there are concerns regarding residual stresses (distortion), microstructural transformation and the formation of cavities/porosity in the weld joint due to the exposure to laser power. These factors are a concern for the mechanical performance of the welded components.

Experimental Technique

Laser beam welding was utilised for joining of 3 mm mill annealed Ti-6Al-4V alloy sheet in a full penetration butt-weld configuration. The sheets chemical composition were: (wt.%) Al 6.25, V 4.04, Fe 0.19, C 0.018, N 0.008, O 0.18 and balance Ti. The welding platform used for this research was a TRUMPF LASERCELL 1005 (TLF laser) based at the National Laser Centre (NLC) in Pretoria, South Africa. Weld coupons for LBW were processed with laser power ranging from 2.3 kW to 4.3 kW and varying traverse speed between 1 m/min and 5 m/min. The weld pool was shielded with Argon gas to reduce oxidation of the weld nugget. The welded plates were cut and sectioned for macrostructure and microstructural evaluation. The samples were mounted and etched using a solution of 2 ml HF (40 %), 5 ml H_2O_2 (30 %) and 10 ml H_2O for approximately 30 seconds. An optical microscope and HR-TEM were used to evaluate the microstructure of the welds. Surface residual stresses were measured using an iXRD Residual Stress Measurement System manufactured by Proto Manufacturing Ltd [11]. The measurements were done on the weld sheets in as as-welded condition. Surface residual stresses were measured along and across the weld, which will represent transverse (sT) and longitudinal stress (sL) respectively. A 3 mm circular aperture was used as it was found that it's the only size that gave a satisfactory resolution and higher peak intensity for this research material. This was attributed to the very fine microstructure of Ti-6Al-4V alloy. A spacing of 1 mm was used for measurements from one point to the next, this allowed for good averaging of data points as an aperture size of 3 mm allowed for an overlap between points. A Bragg angle of 139.69° and 5 Beta oscillations per measurement were used. Copper tube and Nickel filters were used for this research as they are the recommended materials to use when measuring residual stresses for Titanium alloys [11]. For all measurements, an elliptical curve fitting was used for the residual stress data which allowed for the determination of the normal and shear stress components. But only the normal stress component is reported in this research as the shear stress component was found to be very small. The parent plate yield and tensile strength is 890 MPa and 1017 MPa respectively.

Results

There was a flaw-like indications observed in these welds made as show in Table 1. The weld made at welding speed of 1 m/min showed evidence of severe undercut at the weld root. A possible explanation for this is the sudden contraction of the near molten material during cooling of the weld pool. In general, most welds had indications of undercut at the bottom of the weld.

Table 1: Macrographs of welds.

Laser Power [kW]	2.3	3.3			4.3
Welding Speed [m/min]	3	1	3	5	3
Weld cross-section	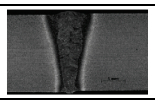	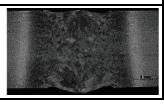	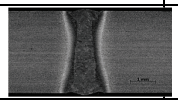	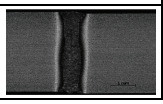	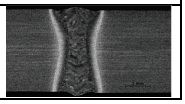

Materials Research Proceedings **4** (2018) 59-64 doi: http://dx.doi.org/10.21741/9781945291678-9

Microstructure

From the optical micrographs, the parent plate showed an α phase in a matrix of retained β phase. The HAZ showed transformed β phase containing acicular α phase. But lower traverse speed resulted in grain growth as compared to high traverse speed. In the weld nugget, low traverse speed resulted in coarse acicular α phase (needle-like α) in prior β grain boundaries while high traverse speed resulted in fine acicular α phase (needle-like α) in prior β grain boundaries. The optical micrographs for the weld zones are illustrated in Table 2. Additionally, the HAZ and weld nugget size varied from wide to narrow as the traverse speed is increased. This was mainly attributed to the cooling rate after the welding process.

Table 2: Indicative optical micrographs for the various weld zones.

Traverse Speed [m/min]	Weld Nugget	Transition Zone	Heat Affected Zone
1	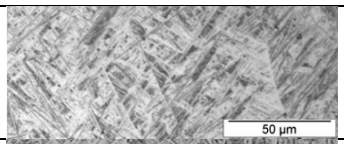	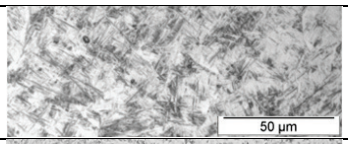	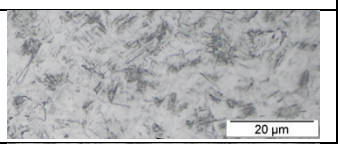
3	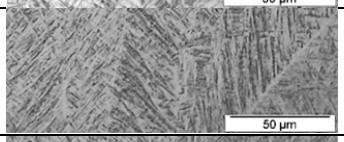	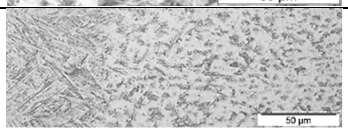	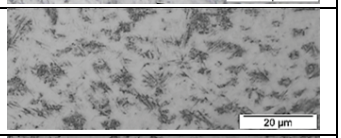
5	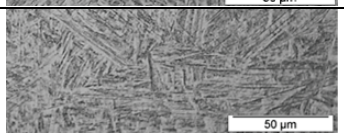	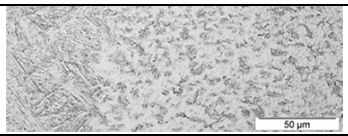	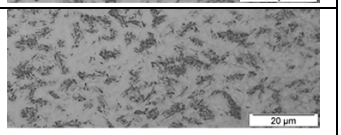

The microstructure was further characterised by placing the samples in the Scanning Electron Microscope (SEM) by first assessing the parent plate to identify the α/β phase distribution of the Ti-6Al-4V alloy. By utilising electron backscatter diffraction (EBSD), the parent plate contained approximately 90 percent α phase (6-10 µm) and about 7 percent retained β phase (1-2 µm). Figure 1 shows the SEM and EBSD images with α phase indicated in blue and β phase in red.

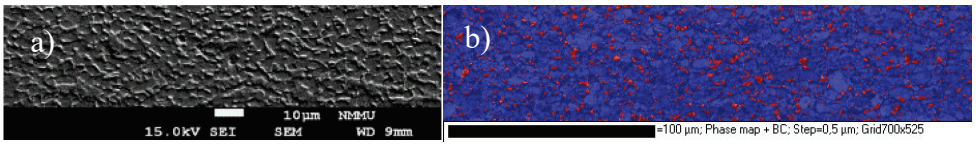

Fig. 1: a) SE SEM images and b) EBSD phase maps (α-blue: β-red) of parent plate.

Further EBSD analysis was done on the welds. The evaluated areas were the weld nugget and the heat affected zones respectively. The weld nugget for all welds showed similar results, there were no traces of β phase irrespective of the traverse speed. Figure 2 to Fig. 3 shows the EBSD phase maps for the welds done. This results are similar to those achieved by Steuwer *et al*. [12] when evaluating the friction stir welded Ti-6Al-4V alloy [12]. Further EBSD analysis was done on the welds. The evaluated areas were the weld nugget and the heat affected zones respectively. The weld nugget for all welds showed similar results, there were no traces of β phase irrespective of the traverse speed. The Scanning Electron Microscope (SEM) was used for crystallographic orientation distribution first for the Ti-6Al-4V alloy parent plate using Electron Backscattered Diffraction (EBSD). The parent plate showed a {0001}<001> plane as the preferred/dominating as shown in Table 3. At low traverse speed, there was no clear preferential

Materials Research Proceedings **4** (2018) 59-64 doi: http://dx.doi.org/10.21741/9781945291678-9

orientation from the HAZ to the weld nugget as indicated in Table 4. Welding direction (WD) is also shown. At intermediate speed, the dominating slip system in the weld nugget and HAZ was between {0001}<001> and {1120}<120> respectively. The weld nugget at high traverse speed showed preferential direction of {1010}<010>. Additionally for both the HAZ and weld nugget, there was evidence of grain growth. The weld nugget at intermediate traverse speed showed prismatic deformation or primary slip at {1120}<120> which has the lowest shear stress compared to basal and pyramidal planes. This slip plane is an indication to have a better performance for fatigue testing.

Table 3: EBSD phase maps (α-blue: β-red) of 3.3 kW at 1 m/min, 3 m/min, 5 m/min for HAZ and Weld Nugget.

Laser Power	Traverse Speed	HAZ	WELD
3.3 [kW]	1 [m/min]		
	3 [m/min]	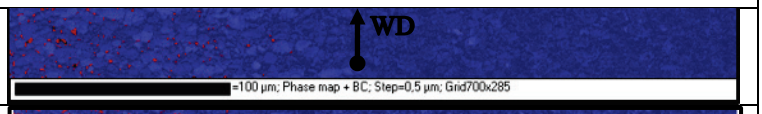	
	5[m/min]	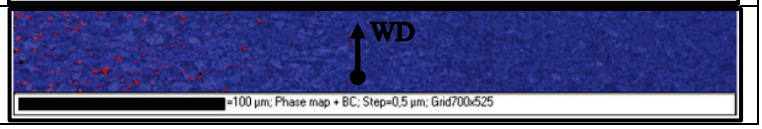	

Table 4: Inverse pole figure map of 3.3 kW at 1 m/min, 3 m/min, 5 m/min for HAZ and Weld Nugget.

Laser Power	Traverse Speed	HAZ	WELD
Parent Plate		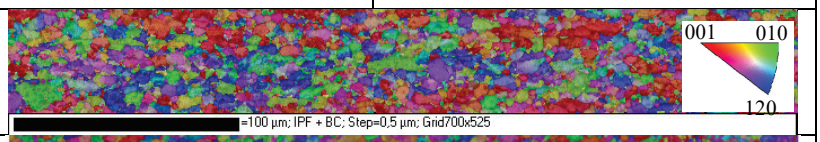	
3.3 [kW]	1 [m/min]	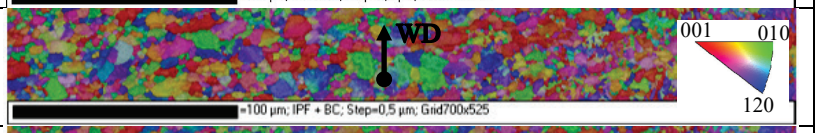	
	3 [m/min]	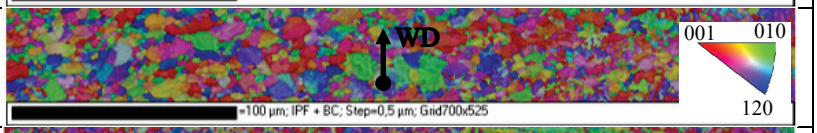	
	5[m/min]	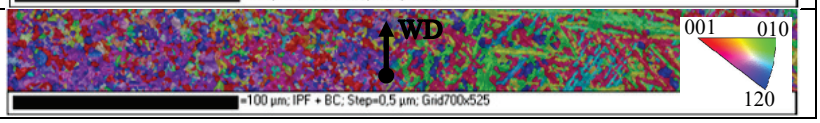	

Surface Residual Stress

The induced residual stresses data in conjunction with microstructural results was used to assist in explaining the effect of traverse speed on weld integrity. Surface Residual Stress data was obtained by X-ray diffraction technique. The measurements were done 40 mm from the center of the weld on each side. From each point measurement, two readings are recorded, that is, longitudinal and transverse stresses. The principle of measuring surface residual stress is based on Bragg's law, which was established by WL Bragg in 1913 [11]. Diffraction only happens when the material measured has a crystalline structure [11].

Residual stresses using diffraction can be calculated using a number methodologies but for this research, the $\sin^2\psi$ method was used as the mostly used method to calculate stress especially at different psi tilts angles [11]. For any given lattice spacing the stress is calculated using Eq. 1:

$$\sigma_\phi = \frac{E}{(1+\nu)sin^2\psi}\left(\frac{d_\psi - d_o}{d_o}\right). \quad (1)$$

Where; σ_ϕ= Single stress acting in a chosen direction i.e. ϕ (MPa), E = Elastic modulus (GPa), ν = Poisson's ratio, ψ = Angle between the normal plane of specimen and normal of the diffracted plane (^{o}), d_o = Inter-planar spacing at free strain (Å) and d_ψ = Inter-planar spacing of planes at angle ψ to the surface (Å). The parent plate was first measured for residual stress. The results revealed that the plates received from the manufacture had the average compressive stresses of 260 ±21 MPa and 160 ±24 MPa in transverse and longitudinal to the rolling directions respectively. The plates were used as received; no normalising of stresses was done for this research. With respect to the weld, longitudinal direction is along the welding direction and transverse direction is perpendicular to the weld direction. The residual stress results showed high tensile stress in the longitudinal direction for all traverse speeds. The highest stresses recorded was 607 ±62 MPa which was at low traverse speed and low stresses of 422 ±29 MPa at high traverse speeds as indicated in Fig. 2a.

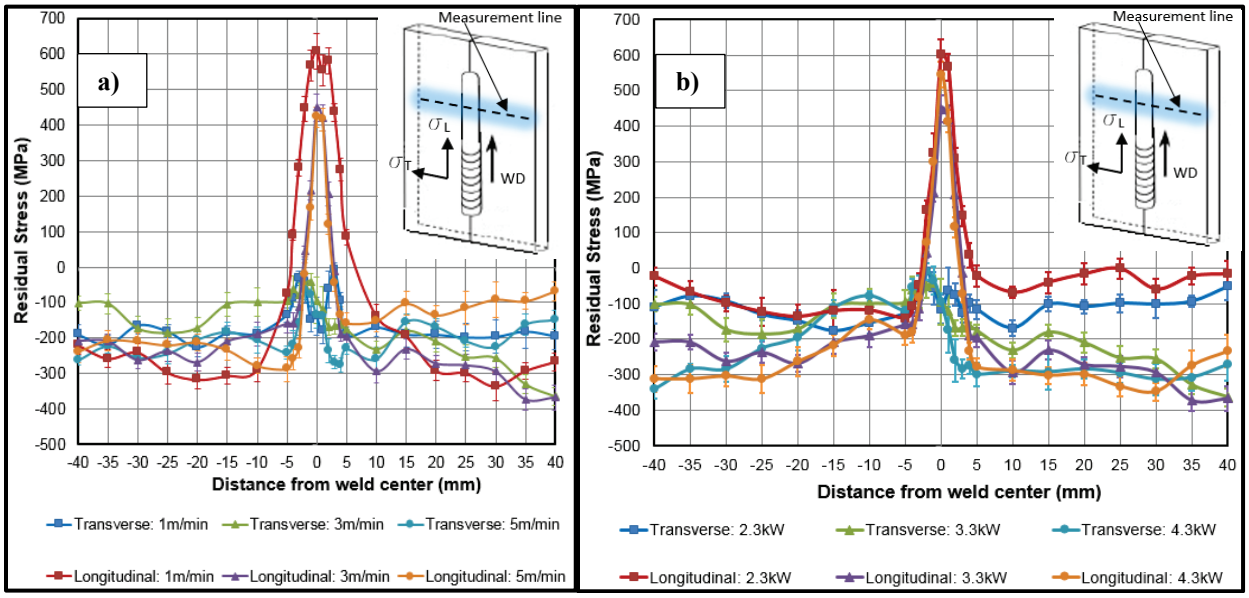

Fig. 2: a) Surface residual stresses for 3.3 kW at 1 m/min; 3 m/min and 5 m/min; b) Surface residual stresses for 3 m/min at 2.3 kW; 3.3 kW and 4.3 kW.

This is as expected at low traverse speed, as the weld nugget becomes wider due to increased time at temperature. There is therefore a larger zone of near molten material in the weld pool. This means that there will be a greater change in width across the weld nugget of a low traverse speed weld versus a high traverse speed weld due to thermal contraction during cooling. This explains why higher residual stresses are found in the weld nugget of low traverse speed welds, even though the low traverse speed welds typically have low cooling rates compared to high cooling rates at high traverse speed. The influence of cooling rate is therefore overwhelmed by the greater influence of thermal contraction of low speeds welds. It therefore follows that as the weld pool cools, a weld with a larger molten pool will experience greater thermal contraction, and hence high residual stresses. Additionally, the transverse direction showed compressive stresses in the range similar to that recorded for the parent plate. Comparing this stresses results with microstructure, it is indicative that the fine microstructure in the weld nugget results in low residual stresses. At traverse speed of 3 m/min, there was no major increase in surface residual

stresses with increased laser power. The highest stress was recorded at 600 ±43 MPa at low laser power of 2.3 kW and lowest stress was 545 ±36 MPa at high laser power of 4.3 kW as illustrated in Fig. 2b.

Conclusion

This research showed that traverse speed has an influence in microstructural transformation. Increased traverse speed resulted in grain growth in the weld nugget and HAZ. The nugget also resulted in fine microstructure. High tensile residual stresses were recorded at low traverse speed but no clear indication of increase /decrease in stresses was recorded with increased laser power. Although there was grain growth and fine microstructure in weld nugget with increased traverse speed, this resulted in reduced residual stresses.

Acknowledgements

The authors wish to give thanks to the staff members from Nelson Mandela University and the NLC situated at the CSIR. The National Research Foundation (NRF) for funding provided.

References

[1] A. O'Brien and C. Guzman, Welding handbook: Welding processes, Part 2, 9th ed., American Welding Society. Miami, 2007.

[2] J.C. Ion, Laser processing of engineering materials: Principles, procedure and industrial application, Elsevier, 2005.

[3] C.T. Dawes, Laser welding: A practical guide, Woodhead Publishing, (1 October 1992).

[4] R. Braun,C. Dalle Donne and G. Staniek, Laser beam welding and friction stir welding of 6013-T6 aluminium alloy sheet. Materialwissenschaft und Werkstoffechnik. 31 (12) (2000) 1017-1026. https://doi.org/10.1002/1521-4052(200012)31:12%3C1017::AID-MAWE1017%3E3.0.CO;2-P

[5] E. Akman, A. Demir, T. Canel and T. Sinmzçlik, Laser welding of Ti6Al4V titanium alloys. J. Mater. Process. Technol. 209 (8) (2009) 3705-3713. https://doi.org/10.1016/j.jmatprotec.2008.08.026

[6] L. Migliore, Welding with lasers. Laser Kinetics. (1998)

[7] L. Reclaru, C. Susz and L. Ardelean, Laser beam welding. Timisoara Medical Journal. 60(1): p. 86-89 (2010)

[8] J. Liu, X.L. Gao, L.J. Zhang and J.X. Zhang, A study of fatigue damage evolution on pulsed Nd:YAG Ti6Al4V laser welded joints. Eng. Fract. Mech. 117 (2014) 84-93. https://doi.org/10.1016/j.engfracmech.2014.01.005

[9] P. Xu, L. Li and S. Zhang, Microstructure characterization of laser welded Ti-6Al-4V fusion zones. Mater. Charact. 87 (2014) 179-185. https://doi.org/10.1016/j.matchar.2013.11.005

[10] H. Liu, K. Nakata and N. Yamamoto, Microstructural characteristics and mechanical properties in laser beam welds of Ti6Al4V alloy. J. Mater. Sci. 47 (2012) 1460-1470. https://doi.org/10.1007/s10853-011-5931-8

[11] PROTO Manufacturing. An introduction x-ray diffraction residual stress measurement. (2011)

[12] A. Steuwer, D.G. Hattingh, M.N. James, U. Singh and T. Buslaps, Residual Stresses, microstructure and tensile properties in Ti-6Al-4V friction stir welds. Sci. Technol. Weld. Joi. 17(7) (2012) 525-533. https://doi.org/10.1179/136217112X13439160184196